Nonadiabatic three-dimensional model of high-order harmonic generation in the few-optical-cycle regime

E. Priori, G. Cerullo,* M. Nisoli, S. Stagira, and S. De Silvestri
Istituto Nazionale per la Fisica della Materia, Centro di Elettronica Quantistica e Strumentazione Elettronica del Consiglio Nazionale della Ricerche, Dipartimento di Fisica, Politecnico di Milano, Piazza Leonardo Da Vinci 32, 20133 Milano, Italy

P. Villoresi, L. Poletto, and P. Ceccherini
Istituto Nazionale per la Fisica della Materia, Laboratorio di Elettronica Quantistica, Dipartimento di Elettronica e Informazione, Università di Padova, Padova, Italy

C. Altucci
Istituto Nazionale per la Fisica della Materia, Dipartimento di Chimica, Università della Basilicata, Potenza, Italy

R. Bruzzese and C. de Lisio
Istituto Nazionale per la Fisica della Materia, Dipartimento di Scienze Fisiche, Università di Napoli Federico II, Napoli, Italy
(Received 30 December 1999; published 5 May 2000)

A numerical model to calculate the high-order harmonics spectrum of a macroscopic gas target irradiated by a few-optical-cycle laser pulse is presented. The single-atom response, calculated within the nonadiabatic strong-field approximation, is the source term of a three-dimensional propagation code. The simulation results show remarkably good agreement with experiments performed in neon using laser pulses with durations of 30 and 7 fs. Both simulations and experiments show discrete and well-resolved harmonics even for the shortest driving pulses.

PACS number(s): 42.65.Ky, 42.65.Re, 32.80−t

I. INTRODUCTION

High-order harmonic generation (HHG) [1,2] is a rapidly developing topic in the field of laser-atom interaction. Besides its fundamental interest, it represents an attractive technique for the production of ultrafast coherent radiation in the UV and soft-x-ray regions of the spectrum using a tabletop system. Recent advances in ultrashort-pulse laser technology have allowed the generation of light pulses with 20–30-fs duration and mJ-level energy; these pulses can be further shortened to sub-10-fs duration by hollow fiber compression [3]. A number of theoretical studies have shown the advantages of using such short pulses for HHG [4–6]; since atoms can be exposed to higher electric fields before a significant fraction is ionized, the conversion efficiency increases and higher energy photoemission can be achieved. In addition, the use of short driving pulses should allow one to combine the fields of several harmonics and generate, under suitable conditions, soft-x-ray pulses with attosecond duration [7]. Recently, several HHG experiments, performed using both 20–30-fs pulses [8–11] and sub-10-fs pulses [12–15], showed a strong dependence of the spectral characteristics of the observed harmonics on the experimental conditions (driving pulse duration and intensity and laser-gas interaction geometry). To understand these results, a detailed theoretical model for the calculation of HHG spectra in the few-optical-cycle regime of the driving pulse is required.

Typical HHG calculations consist of two parts: first the microscopic (single-atom) response to the driving field is calculated, then it is inserted as a source term in the propagation equations of the harmonic field, to obtain the macroscopic response of the excited nonlinear medium. The most accurate way to obtain the single-atom response is the numerical solution of the three-dimensional time-dependent Schrödinger equation [16,17] for the atom interacting with the laser field. Since this approach is quite time consuming, analytical models based on the approximate solution of the Schrödinger equation have been proposed; a particularly successful one, developed by Lewenstein and co-workers [18,19], is known as the strong-field approximation (SFA), and shows good qualitative agreement with the exact solution. When the single-atom response is used to study propagation effects, two approaches are followed. A first set of studies uses the adiabatic approximation, assuming that the atomic response is determined by the instantaneous laser intensity. Using this approach three-dimensional propagation models, calculating the single-atom response either with the Schrödinger equation [20–23] or with the SFA [24–26], have been developed. Other studies use a nonadiabatic approach, calculating for each atom of the nonlinear medium the full response to the electric field of the driving pulse, again using either Schrödinger equation [27–29] or the SFA [30,31]. However, to our knowledge, in the nonadiabatic case, only one-dimensional (plane wave) geometries were considered.

For few-optical-cycle pulses the adiabatic approach is clearly not valid, because the electric field varies considerably during one optical cycle, and the atomic response to the entire pulse (not to an instantaneous intensity) needs to be calculated. On the other hand, in many experimental condi-

*Electronic address: giulio.cerullo@polimi.it

tions, the one-dimensional approximation appears to be too crude.

In this work, we present a three-dimensional propagation model, using the nonadiabatic SFA to calculate the single-atom response. The results of the simulations are compared to the experimental HHG spectra, acquired using 30- and 7-fs pulses. The simulations are in remarkably good agreement with the experimental results, both for the linewidth and relative strength of the harmonics and for the spectral position of the cutoff. The effects of carrier phase on the HHG process are also investigated. The paper is organized as follows: Sec. II introduces the three-dimensional nonadiabatic model used for our calculations. Section III describes the experimental setup and presents the observed harmonic spectra. In Sec. IV the simulation results are discussed and compared to experiments. Finally, Sec. V contains the conclusions.

II. NUMERICAL MODEL

A. Single-atom response

In our numerical model, the single-atom response is calculated using the SFA [18,19], which analytically solves the Schrödinger equation using the following assumptions: (i) all bound states in the atom are neglected, except the ground state; and (ii) in the continuum, the electron is treated as a free particle moving in the laser electric field, with no influence of the atomic potential. This approach has been shown to provide good qualitative agreement with the numerical solution of the Schrödinger equation, at least for harmonic photon energies significantly larger than the atomic ionization potential I_p. In our model the SFA is used in a nonadiabatic form, so that the full electric field of the laser pulse is used to calculate the nonlinear dipole moment (using atomic units) as

$$d_{\mathrm{nl}}(t)=2\,\mathrm{Re}\left\{ i\int_{-\infty}^{t}dt'\left(\frac{\pi}{\varepsilon+i(t-t')/2}\right)^{3/2} \times d^{*}[p_{\mathrm{st}}(t',t)-A(t)]\,d[p_{\mathrm{st}}(t',t)-A(t')] \times \exp[-iS_{\mathrm{st}}(t',t)]E_1(t')\right\}\exp\left[-\int_{-\infty}^{t}w(t')dt'\right]. \tag{1}$$

In Eq. (1), $E_1(t)$ is the electric field of the laser pulse (assumed to be linearly polarized), $A(t)$ is its associated vector potential, ε is a positive regularization constant, p_{st} and S_{st} are the stationary values of the momentum and quasiclassical action, and d is the dipole matrix element for bound-free transitions. The stationary value of momentum is given by

$$P_{\mathrm{st}}(t',t)=\frac{1}{t-t'}\int_{t'}^{t}A(t'')dt'', \tag{2}$$

and the corresponding stationary action is

$$S_{\mathrm{st}}(t',t)=(t-t')I_p-\tfrac{1}{2}p_{\mathrm{st}}^2(t',t)(t-t')+\tfrac{1}{2}\int_{t'}^{t}A^2(t'')dt''. \tag{3}$$

The dipole matrix element for transitions from the ground state to a continuum state characterized by the momentum p can be approximated, for hydrogenlike atoms, as [18]

$$d(p)=i\frac{2^{7/2}(2I_p)^{5/4}}{\pi}\frac{p}{(p^2+2I_p)^3}. \tag{4}$$

The last term in Eq. (1) takes into account ground-state depletion using the theory of Ammosov, Delone, and Krainov [32], which works correctly in our excitation conditions [33], and gives the following tunnel ionization rate from the ground state:

$$w(t)=\omega_p|C_{n*}|^2\left(\frac{4\omega_p}{\omega_t}\right)^{2n^*-1}\exp\left(-\frac{4\omega_p}{3\omega_1}\right), \tag{5}$$

where

$$\omega_p=\frac{I_p}{\hbar},\quad \omega_t=\frac{e|E_1(t)|}{\sqrt{2m_eI_p}},\quad n^*=Z\left(\frac{I_{\mathrm{ph}}}{I_p}\right)^{1/2},$$

$$|C_{n*}|^2=\frac{2^{2n^*}}{n^*\Gamma(n^*+1)\Gamma(n^*)},$$

where Z is the net resulting charge of the atom, I_{ph} is the ionization potential of the hydrogen atom, and e and m_e are electron charge and mass respectively. Equation (5) also provides the free-electron density n_e in the gas, given by

$$n_e(t)=n_0\left\{1-\exp\left[-\int_{-\infty}^{t}w(t')dt'\right]\right\}, \tag{6}$$

where n_0 is the neutral atom density, and only first ionization is considered.

B. Propagation effects

The single-atom response is inserted as a source term into the equations governing the evolution of the fundamental and the harmonic beams, which are solved in cylindrical coordinates and assuming radial symmetry. The propagation of the fundamental wavelength beam in the ionizing gas is described by the equation

$$\nabla^2E_1(r,z,t)-\frac{1}{c^2}\frac{\partial^2E_1(r,z,t)}{\partial t^2}=\frac{\omega_p^2(r,z,t)}{c^2}E_1(r,z,t), \tag{7}$$

where

$$\omega_p(r,z,t)=\left[\frac{e^2n_e(r,z,t)}{\varepsilon_0m_e}\right]^{1/2}$$

is the plasma frequency, z is the propagation coordinate, and r is the transverse coordinate. This equation takes into account both temporal plasma-induced phase modulation and

spatial plasma lensing effects on the fundamental beam, while it does not consider the linear gas dispersion and the depletion of the fundamental beam during the HHG process, which are negligible under our experimental conditions. By going to a moving coordinate frame ($z'=z$ and $t'=t-z/c$) and performing the paraxial approximation (i.e., neglecting $\partial^2 E_1/\partial z'^2$), we obtain the equation

$$\nabla_\perp^2 E_1(r,z',t') - \frac{2}{c}\frac{\partial^2 E_1(r,z',t')}{\partial z'\partial t'} = \frac{\omega_p^2(r,z',t')}{c^2} E_1(r,z',t'). \quad (8)$$

The paraxial approximation, which is valid for beam sizes significantly larger than the wavelength [34], does not impose any limitation on the pulse duration. The temporal derivative in Eq. (8) can be eliminated by a Fourier transform, yielding the equation

$$\nabla_\perp^2 \tilde{E}_1(r,z',\omega) - \frac{2i\omega}{c}\frac{\partial \tilde{E}_1(r,z',\omega)}{\partial z'} = \tilde{G}(r,z',\omega) \quad (9)$$

where

$$\tilde{E}_1(r,z',\omega) = \hat{F}[E_1(r,z',t')],$$

$$\tilde{G}(r,z',\omega) = \hat{F}\left[\frac{\omega_p^2(r,z',t')}{c^2} E_1(r,z',t')\right],$$

and $\hat{F}$ is the Fourier transform operator acting on the temporal coordinate. For the harmonic field we solve the propagation equation

$$\nabla^2 E_h(r,z,t) - \frac{1}{c^2}\frac{\partial^2 E_h(r,z,t)}{\partial t^2} = \mu_0 \frac{\partial^2 P_{\rm nl}(r,z,t)}{\partial t^2}, \quad (10)$$

where $P_{\rm nl}(r,z,t)=[n_0-n_e(r,z,t)]d_{\rm nl}(r,z,t)$ is the nonlinear polarization generated by the gas. In this equation the free-electron dispersion is neglected because the plasma frequency is much lower than the frequencies of high-order harmonics. The nonlinear dipole moment is calculated at each position inside the jet by using the corresponding fundamental field derived by solving Eq. (7). Again going to a moving coordinate frame and using the paraxial approximation, Eq. (10) becomes

$$\nabla_\perp^2 E_h(r,z',t') - \frac{2}{c}\frac{\partial^2 E_h(r,z',t')}{\partial z'\partial t'} = \mu_0 \frac{\partial^2 P_{\rm nl}(r,z',t')}{\partial t'^2}. \quad (11)$$

Also in this case we eliminate the temporal derivative by a Fourier transform, obtaining the equation

$$\nabla_\perp^2 \tilde{E}_h(r,z',\omega) - \frac{2i\omega}{c}\frac{\partial \tilde{E}_h(r,z',\omega)}{\partial z'} = -\omega^2 \mu_0 \tilde{P}_{\rm nl}(r,z',\omega), \quad (12)$$

where $\tilde{E}_h(r,z',\omega)=\hat{F}[E_h(r,z',t')]$ and $\tilde{P}_{\rm nl}(r,z',\omega)=\hat{F}[P_{\rm nl}(r,z',t')]$. Note that in deriving Eqs. (9) and (12) we did not perform the slowly varying envelope approximation in time. These equations are solved, for each value of ω, using a Crank-Nicholson routine. Typical values of the parameters used in the calculation are 2^{12} (for the 7-fs pulses) or 2^{14} (for the 30-fs pulses) points in time, 300 points along the radial direction, and ~400 points along the longitudinal direction. The fundamental pulse is assumed to be Gaussian both in space and in time. Since the longitudinal variations of the fundamental beam over the interaction region (typically of the order of 1 mm) are not too large, we find that it is enough to calculate the source terms in Eqs. (9) and (12) (i.e., $\tilde{G}$ and $\tilde{P}_{\rm nl}$) once every ten steps in the longitudinal direction, thus greatly increasing the speed of the computation. For the harmonic field, gas absorption is also taken into account. Once the harmonic field at the exit face of the gas jet ($z'=z_{\rm out}$) is computed, the power spectrum of the harmonics is obtained by simply integrating over the transverse direction:

$$I_h(\omega) \propto \int_0^\infty |\tilde{E}_h(r,z_{\rm out},\omega)|^2 2\pi r\, dr. \quad (13)$$

Finally, to assess the usefulness of our three-dimensional propagation approach, we also performed calculations using a simpler one-dimensional model. To this purpose we neglected the transverse Laplace operator in Eqs. (9) and (12) and we considered uniform (plane wave) illumination of the target in the transverse dimension. The resulting propagation equations are

$$-\frac{2i\omega}{c}\frac{\partial \tilde{E}_1(z',\omega)}{\partial z'} = \tilde{G}(z',\omega), \quad (14)$$

$$\frac{\partial \tilde{E}_h(z',\omega)}{\partial z'} = -\frac{i}{2} c\omega\mu_0 \tilde{P}_{\rm nl}(z',\omega). \quad (15)$$

In this model the driving-pulse variation along the longitudinal direction are only due to free-electron effects.

III. EXPERIMENT

The experiments reported in this work were performed using a Ti:sapphire laser system with chirped-pulse amplification, generating nearly transform-limited 30-fs pulses, with central wavelength of 795 nm, energy up to 0.8 mJ and 1-kHz repetition rate. These pulses are shortened to sub-10-fs duration using the hollow-fiber compression technique [3,35]. The pulses are first spectrally broadened by propagation into a 60-cm-long hollow fiber, having an inner diameter of 300 μm, filled with argon, and then compressed to an almost transform-limited duration using a high throughput dispersive delay line consisting of six bounces on chirped mirrors [36]; typical pulse durations ranging from 5 to 7 fs are routinely achieved. The spectral broadening in the hollow fiber gives rise to a slight blueshift of the pulse spectrum, with a resulting carrier wavelength of 740 nm. In addition,

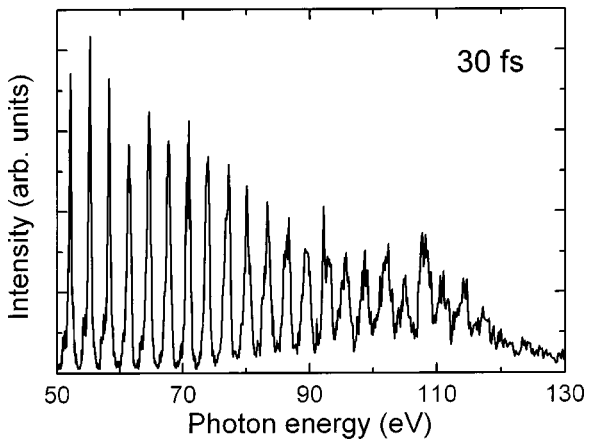

FIG. 1. Measured harmonic emission spectrum of a neon gas jet illuminated by a 30-fs laser pulse with a peak intensity of 7×10^{14} W/cm^2.

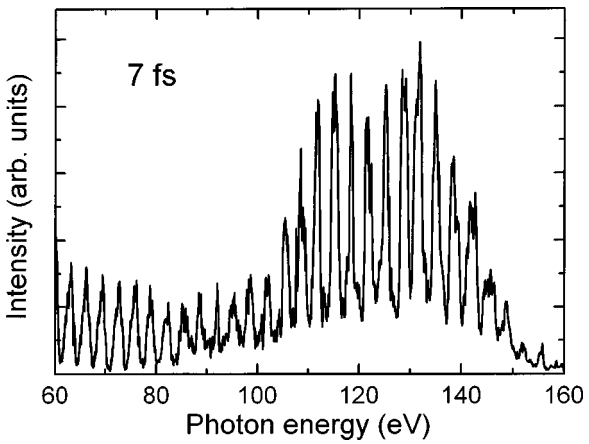

FIG. 2. Measured harmonic emission spectrum of a neon gas jet illuminated by a 7-fs laser pulse with a peak intensity of 9×10^{14} W/cm^2.

the hollow fiber acts as a distributed spatial filter, so that the compressed pulses are diffraction limited and with a nearly Gaussian far-field profile. The sub- 10-fs pulses are focused onto the gas jet by a 25-cm focal length silver mirror and the estimated spot size is $\approx$25 μm (a half-width at $1/e^2$ of intensity). During the experiments we could easily switch from sub- 10-fs to 30-fs excitation pulses by evacuating the hollow fiber, in order to avoid spectral broadening. In this way the spatial properties of the excitation beam remained the same, and the role of the pulse duration could be evaluated.

The gas sample (neon) is injected into the interaction chamber using an electromagnetic valve. The gas pressure at the interaction region, having an estimated length of 1 mm, is approximately 40 torr. The harmonic radiation is analyzed with a grazing-incidence Rowland mounting monochromator designed for broadband efficiency in the 5–50-nm spectral range. A toroidal mirror is used to focus the harmonic beam onto the monochromator entrance slit in the tangential plane. The optical instrument achieves high sensitivity and high spectral resolution (up to 1500), thus allowing a detailed analysis of the spectral structure of the harmonic radiation. The instrumental function was estimated by means of ray tracing of the optical setup in the operative conditions, and taken into account to deconvolute the harmonic linewidths.

Figure 1 shows a typical harmonic spectrum obtained in neon using 30-fs excitation pulses, with the center of the gas jet located $\sim$2 mm downstream the laser beam waist; the estimated laser peak intensity in the interaction region was $\sim7\times10^{14}$ W/cm^2. The spectrum displays well-resolved harmonic peaks at photon energies up to $\sim$130 eV. A typical harmonic spectrum obtained in neon with 7-fs excitation pulses, in the same focalization conditions as the 30-fs pulse and at a laser peak intensity of $\sim9\times10^{14}$ W/cm^2, is shown in Fig. 2. Also in this case we observe discrete and well-resolved harmonic peaks at photon energies up to $\sim$160 eV. The partial overlapping of the harmonic peaks gives rise to a broad pedestal for short wavelengths.

Taking advantage of the well-resolved harmonic spectra for both driving pulses, we have analyzed the wavelength dependence of the harmonic peak linewidths. The experimental results are reported by filled circles in Fig. 3 for 30- (upper panel) and 7-fs (lower panel) driving pulses. The linewidth (at $1/e$ of harmonic peak value) was estimated by fitting the spectral profile of a single harmonic with a Gaussian shape. The contribution of the instrumental function was then quadratically subtracted. The harmonic order dependence of the linewidths is strikingly different in the two situations: For 30-fs pulses, they increase by a factor of 4 in the 50–100-eV energy range, while, for the 7-fs pulses they remain nearly constant with harmonic order.

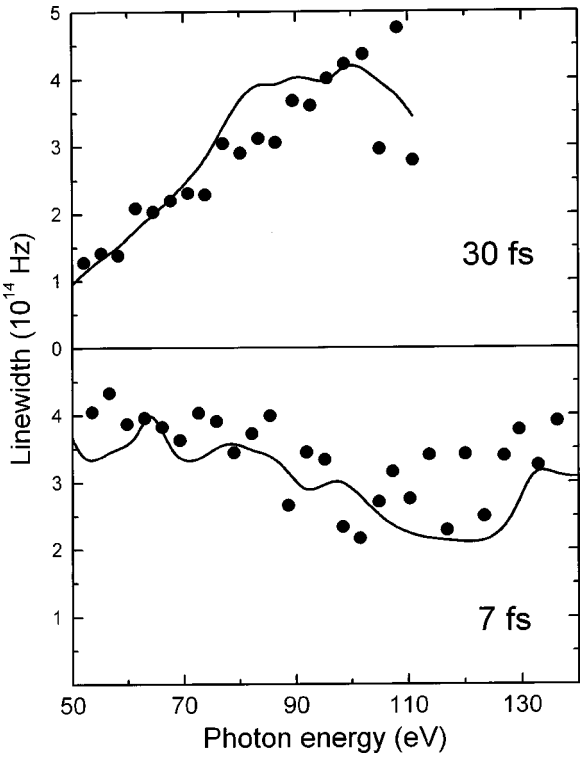

FIG. 3. Linewidths of the harmonics generated by 30-fs (upper panel) and 7-fs (lower panel) pulses. The points represent the experimental data, while the solid lines are the results of simulations using the three-dimensional propagation model.

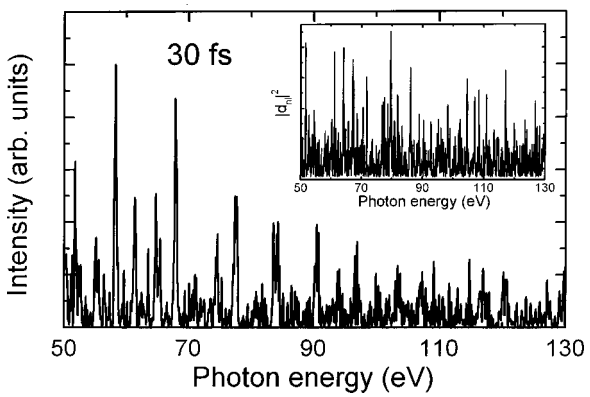

FIG. 4. Macroscopic harmonic spectrum of a neon gas jet, calculated using the one-dimensional propagation model, for a 30-fs driving pulse with a peak intensity of 7×10^{14} W/cm^2. Inset: single-atom emission spectrum.

IV. RESULTS AND DISCUSSION

Single-atom spectra calculated, within the SFA, using 30-fs and 7-fs driving pulses with peak intensities of 7×10^{14} and 9×10^{14} W/cm^2, respectively, are shown in the insets of Figs. 4 and 5. In both cases, the spectra in the plateau region are highly structured, with the individual harmonics hardly recognizable; discrete harmonics reappear only in the vicinity of the cutoff (not shown). The noisy structure of the single-atom emission spectrum in the plateau region is confirmed by the numerical solution of the Schrödinger equation [5,22] and is a typical feature of the short-pulse regime, due to nonadiabatic effects caused by the variation of the driving-pulse intensity over one optical cycle [37]. In fact, a plateau harmonic is made up of two relevant contributions, corresponding to two different electron trajectories in the continuum, which have an intensity-dependent phase [38]. As the laser intensity varies in time, these two contributions are subject to a different frequency shift, leading to a splitting of the harmonic peaks. In ultrashort laser pulses, not only the intensity, but also its time derivative, shows a rapid temporal variation; as a consequence, harmonics emitted over several optical cycles exhibit a broad range of frequency shifts, thus giving rise to highly structured spectra. These results indicate that the single-atom response is not sufficient for the study of the spectral properties of harmonic radiation generated by few-optical-cycle laser pulses.

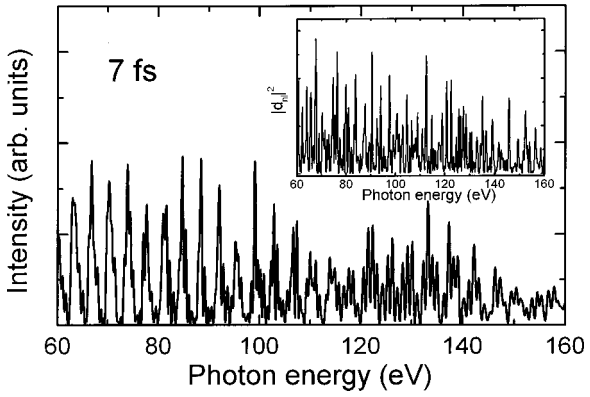

FIG. 5. Macroscopic harmonic spectrum of a neon gas jet, calculated using the one-dimensional propagation model, for a 7-fs driving pulse with a peak intensity of 9×10^{14} W/cm^2. Inset: single-atom emission spectrum.

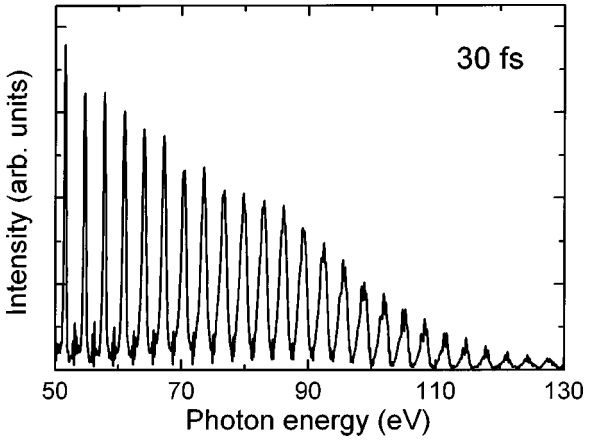

FIG. 6. Macroscopic harmonic spectrum of neon gas jet, calculated using the three-dimensional propagation model, for a 30-fs driving pulse with a peak intensity of 7×10^{14} W/cm^2.

Figures 4 and 5 show HHG spectra obtained from a macroscopic medium (a 1-mm-thick neon jet with uniform atomic density $n_0=1.3\times10^{18}$atoms/cm^3, corresponding to a 40-torr pressure) using the one-dimensional propagation code. The driving pulses have duration of 30 fs (Fig. 4) and 7 fs (Fig. 5), and peak intensities of 7×10^{14} and 9×10^{14} W/cm^2, respectively. Unlike in the single-atom case, harmonics start to become distinguishable, although the spectra are still highly structured and noisy in comparison to the experimental ones. This partial cleanup of the spectra can be attributed to free-electron-induced phase mismatch, which selectively reduces the contribution of some trajectories. For much longer pulses (duration $\approx$150 fs) this mechanism has been shown to be effective in recovering a clean harmonic structure after propagation [30]; in our temporal regime, it cannot explain, alone, the observed features of experimental spectra.

Figure 6 shows a HHG spectrum calculated, using the previously described three-dimensional code, for a 30-fs driving pulse, focused to a waist of 25 μm. The target neon gas jet is located 2 mm downstream from the laser beam waist, has a length of 1 mm and an atomic density, assumed constant along the propagation direction, of $n_0=1.3\times10^{18}$ atoms/cm^3; the laser peak intensity in the center of the jet is 7×10^{14} W/cm^2. These parameters try to reproduce, as closely as possible, the conditions under which the data shown in Fig. 1 were acquired. In this case the spectrum is strikingly different both from the single-atom and one-dimensional spectra, and remarkably similar to the experimental result; it shows discrete and well-resolved harmonics, with widths strongly depending on their order, and very little residual noise between the peaks. This dramatic change in the spectral features can be understood in terms of the phase mismatch mechanisms which are active in three dimensions,

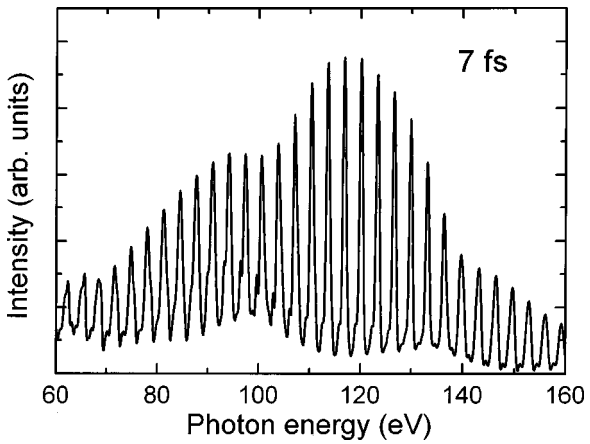

FIG. 7. Macroscopic harmonic spectrum of neon gas jet, calculated using the three-dimensional propagation model, for a 7-fs driving pulse with a peak intensity of $9\times10^{14}\,\mathrm{W/cm^2}$.

in addition to the one induced by free electrons. In fact, in a focused beam, the nonlinear polarization phase depends on longitudinal and radial variations of both intensity and phase of the driving pulse [24,39]: these additional phase mismatch mechanisms lead to a more effective trajectory selection.

Figure 7 shows the harmonic spectrum calculated, with the three-dimensional model, using a few-optical-cycle driving pulse. Its spectral width matches that of the pulse emerging from the hollow fiber, and an additional chirp is introduced to reproduce the experimentally measured pulsewidth of 7 fs. The interaction conditions are the same as in the previous calculation and the pulse peak intensity at the center of the jet is $9\times10^{14}\,\mathrm{W/cm^2}$. Also in this case we obtain good agreement with experimental results (see Fig. 2), and we observe clean and distinct harmonics, due to the same phase-matching mechanisms discussed for the 30-fs pulses. Both calculations and experiments performed using 7-fs pulses clearly demonstrate that, in our interaction geometry, discrete harmonic spectra can be obtained even with sub-10-fs pulses. We also made simulations with transform-limited 5-fs pulses, and still obtained well-resolved harmonics. We note that the previously reported harmonic continuum observed with 5-fs driving pulses [12–14] was obtained using a completely different interaction geometry, with an interaction length one order of magnitude smaller and gas pressures one order of magnitude larger.

Our numerical model also reproduces quite well the wavelength dependence of the harmonic peak linewidths. The estimated linewidths (full width at $1/e$ of the harmonic peak value), obtained from the calculated spectra by fitting the spectral profile of a single harmonic with a Gaussian profile, are shown by solid lines in Fig. 3. Also in this case the agreement with experimental results is very satisfactory. For the 30-fs pulses, the wavelength dependence of the linewidths can be at least partially understood in terms of the different emission times of the harmonics: those well in the plateau are emitted over several optical cycles, while those approaching the cutoff are emitted only over a few cycles, close to the peak intensity of the laser pulse. For the 7-fs driving pulses, the linewidth remains approximately constant with the harmonic order, since all the harmonics are emitted over a few cycles of the driving pulse.

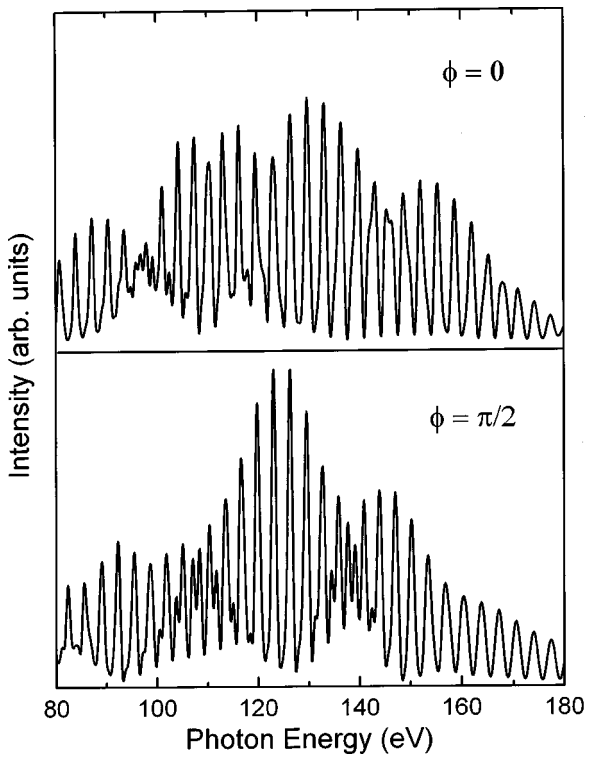

FIG. 8. Macroscopic harmonic spectrum of neon gas jet, calculated using the three-dimensional propagation model, for a 5-fs driving pulse with a peak intensity of $9\times10^{14}\,\mathrm{W/cm^2}$, and two different values of the absolute carrier phase.

For sub-10-fs driving pulses, a strong influence of the carrier phase of the pulse on the single-atom emission spectrum was recently predicted [31,40]. This effect has been pointed out as a limiting factor for the use of few-optical-cycles pulses for HHG, and also proposed as a possible technique for measuring the absolute carrier phase. In order to evaluate its influence in our experimental conditions, we performed simulations with different values of the absolute carrier phase. We found that, for the 7-fs pulses used to simulate our data, the phase has a negligible influence both on the shape and the amplitude of the HHG spectra. We attribute this result to averaging effects due to driving pulse phase variations, both in the longitudinal and transverse directions, which wash out the phase dependence of the single-atom response in the three-dimensional interaction geometry. To study this effect in greater depth, we made simulations with transform-limited 5-fs pulses, for which carrier phase effects should be more pronounced. In these simulations we also neglected free-electron-induced phase modulation, which would reduce the influence of carrier phase. The results are shown in Fig. 8 for two phase values differing by $\pi/2$. In this case we observe some changes in amplitude and shape of the spectra, which, however, do not significantly alter their main characteristics. Our analysis therefore allows us to conclude that macroscopic HHG spectra with sub-10-fs driving pulses do not critically depend, at least in the plateau region, on the absolute carrier phase.

V. CONCLUSIONS

In this work we have presented a numerical model for the calculation of the HHG spectrum emitted by a macroscopic gas target irradiated by an ultrashort laser pulse. The model is nonadiabatic, i.e, the nonlinear dipole moment of each atom in the gas is calculated using the full electric field of the driving pulse; the single-atom response is inserted as a source term in a three-dimensional propagation code, which fully includes plasma effects on the fundamental wavelength beam. The nonadiabatic approach is obviously needed for few-optical-cycle pulses; our work shows that, in our interaction geometry, only a three-dimensional calculation can reproduce satisfactorily the experimental results. We find that, while the single-atom emission spectra are highly structured and noisy in the plateau, after propagation they are considerably cleaned and recover a discrete and well-resolved harmonic structure. Comparing our simulations to experimental results obtained focusing on neon pulses with duration ranging from 30 to 7 fs we find remarkably good agreement, both for the linewidth and relative strength of the harmonics and for the spectral position of the cutoff. It is interesting to note that, even with 7-fs driving pulses, both simulations and experimental results show discrete and well resolved harmonics.

The model provides a tool for studying the physics of HHG using few-optical-cycle driving pulses, and enables one to investigate a number of topics (e.g., the effects of carrier phase on harmonic spectra) under realistic experimental conditions. In addition, it will allow one to study the transverse properties of the emitted harmonics and their focusability, which is an important issue for applications to soft-x-ray nonlinear optics.

ACKNOWLEDGMENT

This study was partially supported within the framework of the Istituto Nazionale di Fisica della Materia under the project ''Femtosecond soft x-ray generation by high energy laser pulses.''

[1] A. L'Huillier and P. Balcou, Phys. Rev. Lett. **70**, 774 (1993).
[2] J. J. Macklin, J. D. Kmetec, and C. L. Gordon III, Phys. Rev. Lett. **70**, 766 (1993).
[3] M. Nisoli, S. De Silvestri, and O. Svelto, Appl. Phys. Lett. **68**, 2793 (1996).
[4] I. P. Christov, J. Zhou, J. Peatross, A. Rundquist, M. M. Murnane, and H. C. Kapteyn, Phys. Rev. Lett. **77**, 1743 (1996).
[5] K. J. Schafer and K. C. Kulander, Phys. Rev. Lett. **78**, 638 (1997).
[6] C. Kan, N. H. Burnett, C. E. Capjack, and R. Rankin, Phys. Rev. Lett. **79**, 2971 (1997).
[7] P. Antoine, A. L'Huillier, and M. Lewenstein, Phys. Rev. Lett. **77**, 1234 (1996).
[8] J. Zhou, J. Peatross, M. M. Murnane, H. C. Kapteyn, and I. P. Christov, Phys. Rev. Lett. **76**, 752 (1996).
[9] Z. Chang, A. Rundquist, H. Wang, M. M. Murnane, and H. C. Kapteyn, Phys. Rev. Lett. **79**, 2967 (1997).
[10] H. J. Shin, D. G. Lee, Y. H. Cha, K. H. Hong, and C. H. Nam, Phys. Rev. Lett. **83**, 2544 (1999).
[11] C. Altucci, R. Bruzzese, C. de Lisio, M. Nisoli, S. Stagira, S. De Silvestri, O. Svelto, P. Ceccherini, L. Poletto, G. Tondello, and P. Villoresi, Phys. Rev. A (to be published).
[12] Ch. Spielmann, N. H. Burnett, S. Sartania, R. Koppitsch, M. Schnürer, C. Kan, M. Lenzner, P. Wobrauschek, and F. Krausz, Science **278**, 661 (1997).
[13] Ch. Spielmann, C. Kan, N. H. Burnett, T. Brabec, M. Geissler, A. Scrinzi, M. Schnürer, and F. Krausz, IEEE J. Sel. Top. Quantum Electron. **4**, 249 (1998).
[14] M. Schnürer, Z. Cheng, M. Hentschel, G. Tempea, P. Kálmán, T. Brabec, and F. Krausz, Phys. Rev. Lett. **83**, 722 (1999).
[15] M. Nisoli, S. Stagira, G. Cerullo, S. De Silvestri, O. Svelto, P. Ceccherini, L. Poletto, G. Tondello, P. Villoresi, C. Altucci, R. Bruzzese, and C. de Lisio, Appl. Phys. B, submitted.
[16] J. L. Krause, K. J. Schafer, and K. C. Kulander, Phys. Rev. A **45**, 4998 (1992); Phys. Rev. Lett. **68**, 3535 (1992).
[17] I. P. Christov, M. M. Murnane, and H. C. Kapteyn, Phys. Rev. Lett. **78**, 1251 (1997).
[18] M. Lewenstein, Ph. Balcou, M. Yu. Ivanov, A. L'Huillier, and P. B. Corkum, Phys. Rev. A **49**, 2117 (1994).
[19] P. Salieres, A. L'Huillier, P. Antoine, and M. Lewenstein, Adv. At., Mol., Opt. Phys. **41**, 83 (1998).
[20] A. L'Huillier, Ph. Balcou, S. Candel, K. J. Schafer, and K. C. Kulander, Phys. Rev. A **46**, 2778 (1992).
[21] A. L'Huillier, K. J. Schafer, and K. C. Kulander, J. Phys. B **24**, 3315 (1991).
[22] M. B. Gaarde, Ph. Antoine, K. J. Schafer, K. C. Kulander, and A. L'Huillier, Phys. Rev. A **57**, 4553 (1998).
[23] M. B. Gaarde, F. Salin, E. Constant, Ph. Balcou, K. J. Schafer, K. C. Kulander, and A. L'Huillier, Phys. Rev. A **59**, 1367 (1999).
[24] P. Salieres, A. L'Huillier, and M. Lewenstein, Phys. Rev. Lett. **74**, 3776 (1995).
[25] P. Antoine, A. L'Huillier, M. Lewenstein, P. Salieres, and B. Carrè, Phys. Rev. A **53**, 1725 (1996).
[26] Ph. Antoine, D. B. Milosevic, A. L'Huillier, M. B. Gaarde, P. Salieres, and M. Lewenstein, Phys. Rev. A **56**, 4960 (1997).
[27] I. P. Christov, M. M. Murnane, and H. C. Kapteyn, Phys. Rev. A **57**, R2285 (1998).
[28] S. C. Rae and K. Burnett, J. Phys. B **26**, 1509 (1993).
[29] S. C. Rae, K. Burnett, and J. Cooper, Phys. Rev. A **50**, 3438 (1994).
[30] C. Kan, C. E. Capjack, R. Rankin, and N. H. Burnett, Phys. Rev. A **52**, R4336 (1995).
[31] G. Tempea, M. Geissler, and T. Brabec, J. Opt. Soc. Am. B **16**, 669 (1999).
[32] M. V. Ammosov, N. B. Delone, and V. P. Krainov, Zh. Eksp. Teor. Fiz. **91**, 2008 (1986) [Sov. Phys. JETP **64**, 1191 (1986)].
[33] D. Bauer and P. Mulser, Phys. Rev. A **59**, 569 (1999).
[34] A. E. Siegman, *Lasers* (Cambridge University, Oxford, 1986), Sec. 16.1.
[35] M. Nisoli, S. Stagira, S. De Silvestri, O. Svelto, S. Sartania, Z.

Cheng, G. Tempea, Ch. Spielmann, and F. Krausz, IEEE J. Sel. Top. Quantum Electron. **4**, 414 (1998).

[36] G. Tempea, F. Krausz, Ch. Spielmann, and K. Ferencz, IEEE J. Sel. Top. Quantum Electron. **4**, 193 (1998).

[37] F. M. Kien, K. Midorikawa, and A. Suda, Phys. Rev. A **58**, 3311 (1998).

[38] M. Lewenstein, P. Salieres, and A. L'Huillier, Phys. Rev. A **52**, 4747 (1995).

[39] P. Balcou, P. Salieres, A. L'Huillier, and M. Lewenstein, Phys. Rev. A **55**, 3204 (1997).

[40] A. de Bohan, P. Antoine, D. B. Milosevic, and B. Piraux, Phys. Rev. Lett. **81**, 1837 (1998).